

# Combining remote sensing imagery and forest age inventory for biomass mapping

G. Zheng<sup>a,\*</sup>, J.M. Chen<sup>b</sup>, Q.J. Tian<sup>a</sup>, W.M. Ju<sup>b</sup>, X.Q. Xia<sup>a</sup>

<sup>a</sup>International Institute for Earth System Science, Nanjing University, Nanjing 210093, China

<sup>b</sup>Department of Geography and Program in Planning, University of Toronto, 100 Street George Street, Room 5047, Toronto, Ont., Canada M5S 3G3

Received 7 June 2005; received in revised form 26 March 2006; accepted 25 July 2006

Available online 28 November 2006

## Abstract

Aboveground biomass (AGB) of forests is an important component of the global carbon cycle. In this study, Landsat ETM<sup>+</sup> images and field forest inventory data were used to estimate AGB of forests in Liping County, Guizhou Province, China. Three different vegetation indices, including simple ratio (SR), reduced simple ratio (RSR), and normalized difference vegetation index (NDVI), were calculated from atmospherically corrected ETM<sup>+</sup> reflectance images. A leaf area index (LAI) map was produced from the RSR map using a regression model based on measured LAI and RSR. The LAI map was then used to develop an initial AGB map, from which forest stand age was deduced. Vegetation indices, LAI, and forest stand age were together used to develop AGB estimation models for different forest types through a stepwise regression analysis. Significant predictors of AGB changed with forest types. LAI and NDVI were significant predictors of AGB for Chinese fir ( $R^2 = 0.93$ ). The model using LAI and stand age as predictors explained 94% of the AGB variance for coniferous forests. Stand age captured 79% of the AGB variance for broadleaved forests ( $R^2 = 0.792$ ). AGB of mixed forests was predicted well by LAI and SR ( $R^2 = 0.931$ ). Without differentiating among forest types, the model with SR and LAI as predictors was able to explain 90% of AGB variances of all forests. In Liping County, AGB shows a strong gradient that increases from northeast to southwest. About 64% of the forests have AGB in the range from 90 to 180 t ha<sup>-1</sup>.

© 2006 Published by Elsevier Ltd.

**Keywords:** Stand age; Aboveground biomass; Remote sensing; Vegetation index

## 1. Introduction

For climate change research, it is important to know how much net CO<sub>2</sub> is released to the atmosphere from terrestrial ecosystems (IPCC, 1996). Forest ecosystems are an important component in the terrestrial ecosystems that exchange CO<sub>2</sub> with the atmosphere. Forest biomass resulting from the long-term accumulation of carbon (C) is an important part of the C cycle. In modeling the C balance of terrestrial ecosystems, biomass is often required as an input to models because it affects autotrophic respiration and the amount of C transferred to the soil as litter.

In recent decades, efforts have been made to estimate forest biomass, including field measurements and model

simulations. For example, Xu (1999) presented a model for estimating biomass from the diameter-at-breast height (DBH), tree height, crown size, crown length, and crown volume. Measurements of these parameters are time- and labour-consuming, thus limiting use of this approach over large areas. Other scientists calculated biomass using traditional methods such as the dry-weighted algorithm (Haripriya, 2000; Jing-Yun Fang et al., 1998).

Due to its large spatial and frequent temporal coverage, remote sensing allows scientists to examine properties and processes of ecosystems and their inter-annual variability at multiple scales (Goetz et al., 2000; Prince and Goward, 1995; Running et al., 2000; Zheng et al., 2004). It has been demonstrated that the Landsat ETM<sup>+</sup> imagery is very useful in forest management when combined with field measurements (Dorren et al., 2003). The spectral information detected by remote sensing has a good correlation with

\*Corresponding author. Tel.: +86 25 83597351; fax: +86 25 83592288.  
E-mail address: zhengguang1982@163.com (G. Zheng).

forest biomass (Spencer et al., 1997). Forest biomass depends on the land cover, canopy chlorophyll content and forest density, all of which influence spectral reflectance recorded by satellite sensors). Recently, data from radar remote sensing was also used to estimate the aboveground biomass (AGB) (Moreau and Le Toan, 2003; Rauste, 2005).

Some remote sensing-based biomass models consider processes of radiative transfer in plant canopies such as the absorption, reflection, and transmission of solar radiation in the canopy which are related to biomass. Statistical models can also be developed using remotely sensed information and ecological factors. The accuracy of these biomass models using remote sensing data has been questioned (Zhang and Fu, 1999) because in reality, optical remote sensing provides information on canopy leaf density rather than on biomass. Biomass may therefore be estimated from parameters quantifying canopy density, such as LAI.

In practical remote sensing applications, LAI is calculated from remotely sensed vegetation indices through regression analysis or the inversion of geometric radiation models. Since the saturation of vegetation indices often caused the underestimation of high LAI values (Gitelson, 2004), remotely sensed LAI alone is unable to give reliable estimates of biomass. Therefore, other parameters, such as stand age and forest type, are also required for the retrieval of AGB.

The objectives of this study are: (1) to develop an algorithm for estimating AGB from remote sensing data; and (2) to produce a high-resolution AGB map for further modeling net primary productivity (NPP) and C balance for Liping County, Guizhou Province, China.

## 2. Materials and methods

### 2.1. Study area

Liping County (25°44'–26°31'N, 108°37'–109°31'E) is located in the southeast of Guizhou Province, China. This area represents the transition from Yunnan-Guizhou altiplano to Guangxi Zhuang Autonomous Region, and to Hunan low mountains and hills. It is a typical karst area in south China (Fig. 1), with an elevation generally ranging between 600 and 800 m above sea level (asl). The highest peak of Laoshan circle is 1598 m asl. The entire area falls within the monsoon moist climate area of the middle subtropical zone. Annual rainfall ranges from 1100 to 1700 mm. Forest unevenly distributes in its 29 villages and towns. The total forested land area is 371,934.8 ha, accounting for 83.78% of its total land area (444,288.7 ha) and 58.44% of the whole territory of the Liping County. Among these forests, 16.22% are difficult to utilize. Forest species are abundant with 76 families, 224 genus, and 521 species, including 24 state-protected species. The four major species are China fir, pine, tea-oil camellia, and bamboo. Coniferous forests occupy 43.36% of the forested areas.

### 2.2. Methods

In this study, we employed various methods to measure ecological parameters, to process remote sensing images, and to develop regression models for calculating biomass from remotely sensed information.

During the field campaign, topographic characteristics (slope, aspect, coordinates) and vegetation parameters

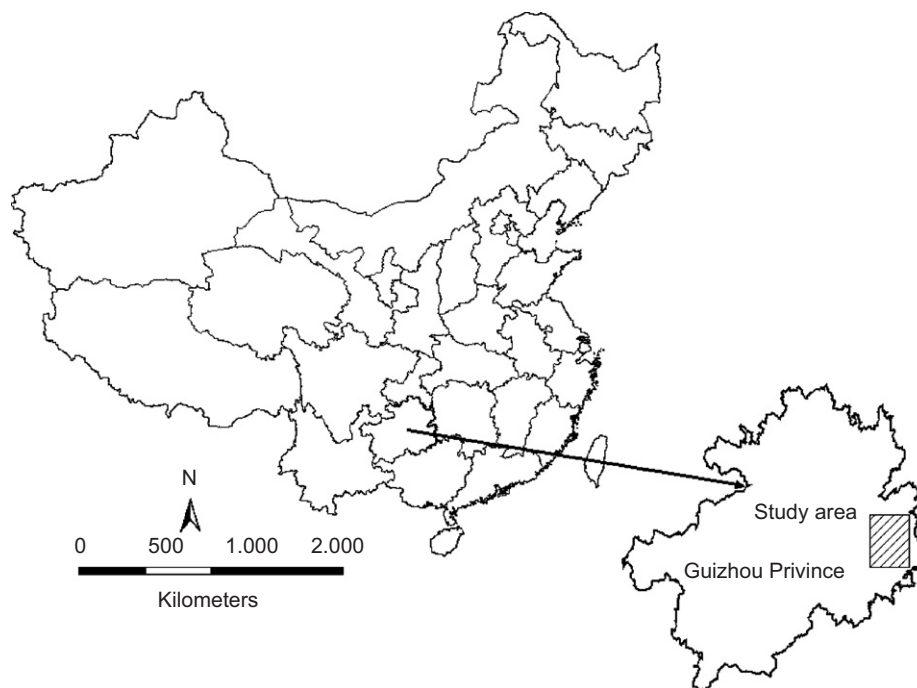


Fig. 1. The location of study area indicates the dependent which participate in the regression model building.

(LAI, DBH, tree height, forest age) were measured. Forest biomass was calculated by the relative-growth method, for which the necessary parameters are available easily and effectively, and a great deal of studies done in China prove that it is very useful and practical. Three vegetation indices, including normalized difference vegetation index (NDVI), simple ratio (SR), and reduced simple ratio (RSR), were calculated from remotely sensed reflectance in the red, near infrared and shortwave infrared ETM<sup>+</sup> bands. A LAI map was produced using a RSR-based algorithm developed according to measured LAI and remotely sensed RSR values. The relationship between AGB and LAI was analyzed to calculate AGB values from the LAI map. Based on this initial AGB map, stand age was deduced using a forest age estimation model with AGB as the input. Finally, three vegetation indices, LAI, and stand age were used to develop AGB models for different forest types. From these models and maps of vegetation indices, LAI, and stand age, a final AGB map was produced. The major steps in mapping AGB from remote sensing and inventory data are shown in Fig. 2.

### 2.3. Field measurements and biomass estimation

Field campaigns were conducted in August 2003 and 2004. In total, 60 plots of mason pine, Chinese fir and mixed forest plantations were investigated. At each plot, LAI and soil measurements were made. LAI was measured

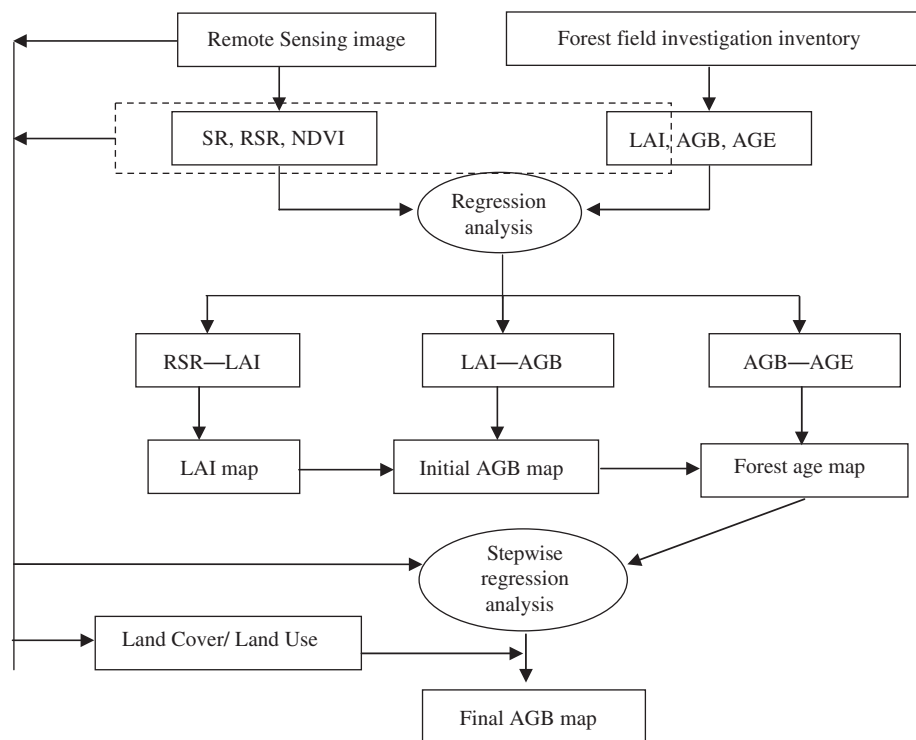
with a fish-eye camera and TRAC (Chen and Cihlar, 1995). Topographic parameters (slope, aspect) were also measured. The latitude and longitude of each plot were recorded with a high-accuracy global positioning system (GPS). Parameters required to calculate AGB were observed at 14 among the 60 plots only, including tree height and the annual tree ring increment at the breast height from tree core samples taken from about 10 trees at each plot. For each sampled tree, ABG was calculated from DBH and tree height, i.e.

$$AGB = a(D^2H)^b, \quad (1)$$

where  $D$  and  $H$  are, respectively, the DBH and tree height;  $a$  and  $b$  are regression parameters. Eq. (1) was previously used to estimate AGB for Chinese fir, mason pine and other forests in areas close to Liping County by others (Feng et al., 1999). The biomass of each physiological organ was first calculated and summed up to get the AGB value of a tree. The AGB value of a plot is the average of AGB values of all sampled trees.

### 2.4. Remote sensing data processing and vegetation index calculation

Two ETM<sup>+</sup> images acquired on May 14 and 21, 2000 were employed in the study. Using gain and offset coefficients included in the header files, the ETM<sup>+</sup> raw digital numbers were first converted into radiance, from



----- Indicates the dependent which participate in the regression model building

Fig. 2. Flow chart of mapping aboveground biomass from remote sensing and field forest inventory data. Variables in the dashed line box are used to set up regression models.

which the reflectance of each band (except the thermal and panchromatic bands) was calculated using the “6S” model (Vermeote et al., 1997). Next, reflectance images from the 2 days were joined to produce a reflectance image for the whole study area. The boundary of Liping County was then overlaid to exclude pixels outside the study area. All images were geo-rectified to the UTM projection.

Liping County is a typical area with hills and varying terrain. Topography thus imposes considerable noise on remote sensing signals, as terrain shadows reduce reflectance and cause errors in derived vegetation parameters. The removal of this shadow effect was implemented by the Sun-Canopy-Sensor (SCS) sub-pixel removal method (Degui Gu, 1998), which is suitable for forest mapping using Landsat ETM<sup>+</sup>. This method quantifies the, parameterizes the interaction between solar radiation and vegetated sloping terrain.

Three vegetation indices (NDVI, SR, RSR) were calculated from the reflectance image, i.e.

$$NDVI = (NIR - Red)/(NIR + Red), \tag{2a}$$

$$SR = (NIR/Red), \tag{2b}$$

$$RSR = SR \left[ 1 - \frac{(SWIR - SWIR_{min})}{(SWIR_{max} - SWIR_{min})} \right], \tag{2c}$$

where NDVI, SR and RSR are, respectively, NDVI, SR and RSR; NIR, Red, and SWIR are surface reflectance values in the red, near infrared, and shortwave infrared

bands; and SWIR<sub>min</sub> and SWIR<sub>max</sub> are the minimum and maximum values in the shortwave infrared reflectance (taken as 1% cutoff points in the reflectance histogram).

The minimum and maximum SWIR values correspond to reflectance by a completely closed canopy and an open canopy. It has been shown that RSR has advantages of reducing the effect of background reflectance, increasing sensitivity to LAI changes, and reducing the differences between deciduous and coniferous species in LAI retrieval algorithms (Brown et al., 2000).

2.5. LAI, land cover, initial AGB, and stand age maps

Measurements of LAI and calculated RSR were used to build a statistical model for calculating LAI. Based on this model and the RSR map, a LAI map of Liping County was produced. This LAI map was employed for estimating the initial values of AGB according to the observed relationship between LAI and AGB. The initial AGB map was further used to deduce stand age, which is an input to the model calculating the final values of AGB.

Land cover is a very important factor in mapping AGB. The land cover was classified into two steps. The NDVI map was first used to classify forested and non-forested pixels through setting a NDVI threshold. Subsequently, forests were further classified into four categories (broadleaf, coniferous, mixed forests and bamboo) through parallelepiped supervised classification. Mixed and coniferous forests are the major forest types in the area (Fig. 3).

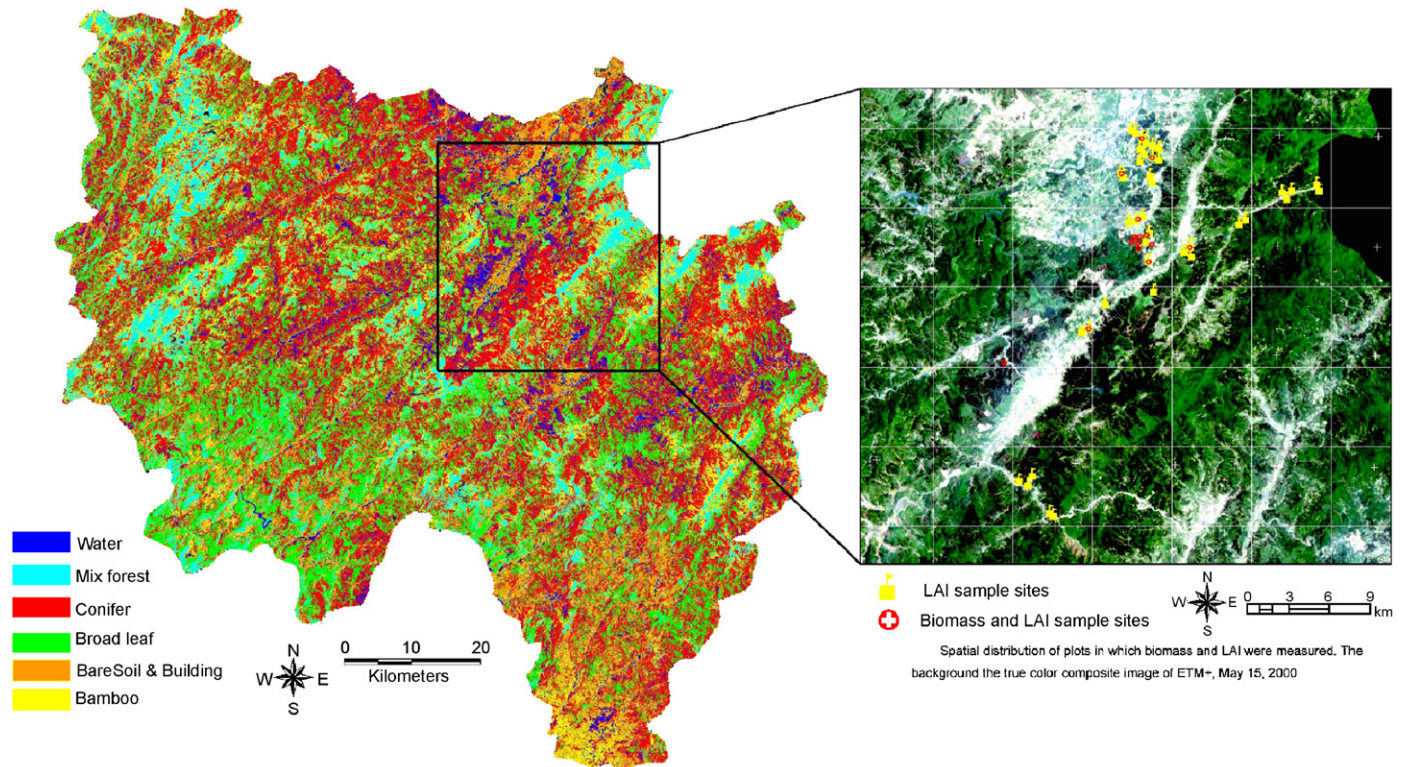


Fig. 3. Land cover map and LAI and AGB sites of Liping County.

### 3. Results

#### 3.1. Correlation between AGB and LAI

In this study, AGB is defined as the biomass of live trees greater than 3.0 cm in DBH and taller than 1.3 m. Measured LAI has a good relationship with AGB calculated from DBH and tree height at the plot level ( $R^2 = 0.6099$ ,  $N = 14$ ). When LAI is below 4.5, AGB increases linearly with LAI. For plots with LAI larger than 4.5, the correlation between AGB and LAI was less significant (Fig. 4). This model was used to estimate

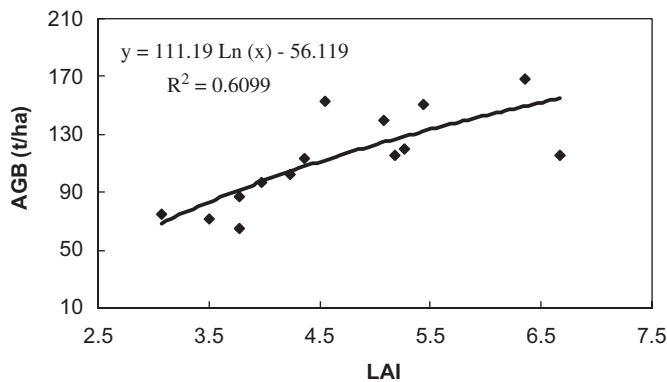


Fig. 4. The relationship between aboveground biomass and leaf area index measured at 14 plots.

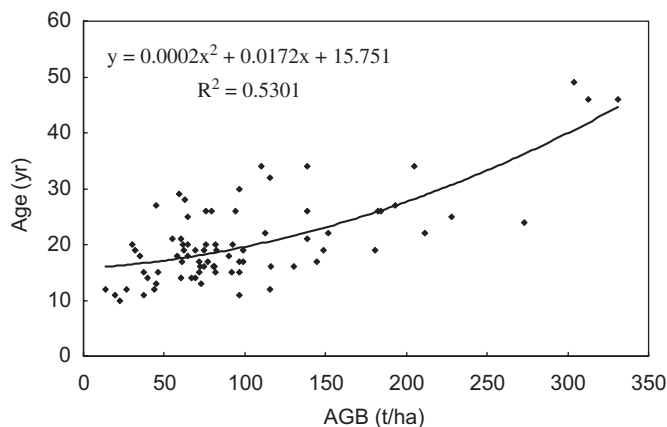


Fig. 5. The relationship between AGB and age of trees.

AGB from the LAI map. However, the AGB value calculated from LAI has considerable uncertainties due to the insensitive response of AGB to high LAI values above 4.5. Therefore, AGB calculated in this way was considered as the initial AGB. In the initial AGB map (Fig. 5), the inferred AGB had a low spatial variation as the AGB of most forests ranged from 40 to 100 t ha<sup>-1</sup>. The value of the initial AGB map was to provide input to deducing stand age, which would be used as a predictor for the final estimate of AGB.

#### 3.2. The relationship between tree age and AGB

Tree age is closely related to its AGB. A second-order polynomial model with AGB as the predictor could explain 53% of age variance for the 60 sampled trees (Fig. 5); it is evident that AGB increases nonlinearly with stand age. The polynomial model was employed to infer stand age from the initial AGB map. Most of the forests were less than 21 yr old in 2004. The age map provides useful information about the forest age structure, not only for mapping AGB but also for managing forest and estimating C balance of forested ecosystems (Chen et al., 2003).

#### 3.3. Models for estimating AGB

Three vegetation indices, LAI, and stand age were used as predictors to build AGB prediction models for different forest types using the stepwise regression method. Table 1 shows predictors selected in each model and the variance in AGB explained. LAI and NDVI are significant predictors of AGB for Chinese fir ( $R^2 = 0.93$ ,  $N = 8$ ). The model using LAI and stand age as inputs explained 94% of AGB variance for coniferous forest ( $N = 11$ ). Stand age accounted for 79% of AGB variance for broadleaved forest ( $N = 5$ ). AGB of mixed forest was well predicted by LAI and SR ( $R^2 = 0.931$ ,  $N = 3$ ). This model explained 90% of AGB variations. Stand age and land cover were therefore factors contributing improved AGB calculation.

Due to the limitations of field measurements, the number of sites with all measured parameters was insufficient for a complete model validation. 26 sampled trees were randomly chosen for model validation of each tree predicted by models in Table 1 were compared with those calculated from measured DBH and tree height using Eq. (1). In the

Table 1  
Models based on stepwise regressions for predicting aboveground biomass from vegetation indices, LAI and stand age

Descriptions	Models	$R^2$
Overall	$AGB = 43.351 * LAI + 4.443 * AGE - 166.565$	0.895
Chinese fir	$AGB = 36.941 * LAI + 197.411 * NDVI - 125.951$	0.930 ( $n = 8$ )
Conifer	$AGB = 55.185 * LAI + 3.862 * AGE - 204.038$	0.937 ( $n = 11$ )
Broadleaf	$AGB = 7.238 * AGE - 15.792$	0.792 ( $n = 5$ )
Mix forest	$AGB = 26.808 * LAI + 15.181 * SR - 60.584$	0.931 ( $n = 3$ )

estimation of AGB, plot means of measured LAI, calculated vegetation indices, and measured tree age were used to drive the model. 91% of the AGB variance among the 26 trees was captured by the model; however, high AGB values were slightly underestimated (Fig. 6).

3.4. Spatial distribution of modeled AGB

Using the AGB model for each forest type, the final AGB map was created (Fig. 7). In Liping County, forest

AGB shows a definite gradient increasing from the northeast to the southwest. Forests in areas close to roads, rivers, and towns usually have AGB less than 40 t ha<sup>-1</sup>. In the southwestern part, AGB values are fairly high, ranging from 120 to 200 t ha<sup>-1</sup>.

About 64% of forests have AGB between 90 and 180 t ha<sup>-1</sup> (Fig. 8). AGB values of 46.3% of forests range from 90 to 120 t ha<sup>-1</sup>. The frequency distribution of AGB values in the final AGB map is very similar to that of measured tree AGB values (Fig. 8).

Values in the initial AGB map, which was produced using LAI only, are clustered in the range from 41 to 60 t ha<sup>-1</sup> (Fig. 8). Overall, AGB in the initial AGB map was significantly underestimated, as only a few stands had AGB above 140 t ha<sup>-1</sup>, showing that the AGB range in the initial map does not represent the reality. In the final AGB map, about 28% of AGB values are above 140 t ha<sup>-1</sup>.

4. Conclusions and discussion

In this study, AGB models for different forest types were developed to calculate AGB values with the aid of remotely sensed forest parameters. The results clearly show that inclusion of stand age and land cover in AGB can effectively improve the accuracy of AGB estimation. Nevertheless, some issues remain to be addressed. In this study, the stand age map was inferred from the initial

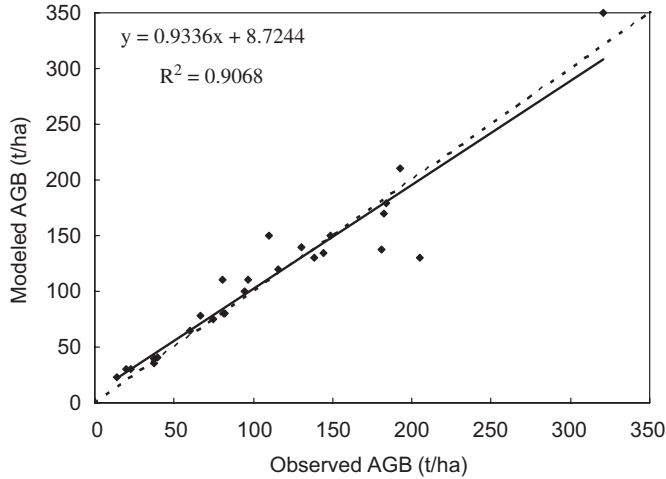


Fig. 6. Validation of modeled AGB against measured AGB.

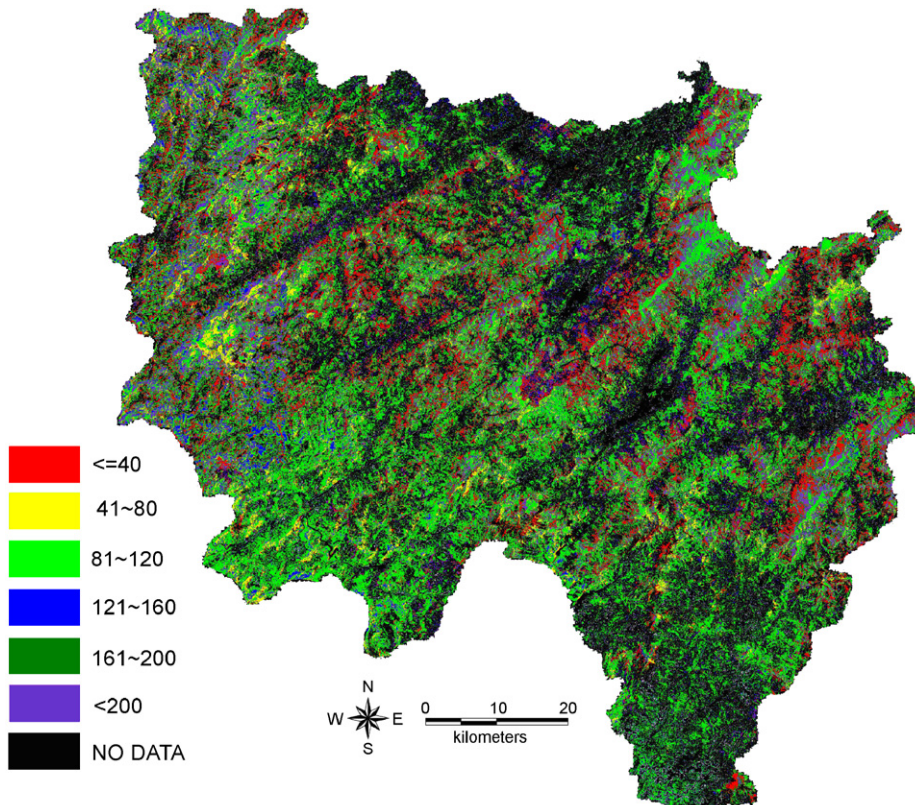


Fig. 7. Spatial distribution of mapped final aboveground biomass for Liping County.

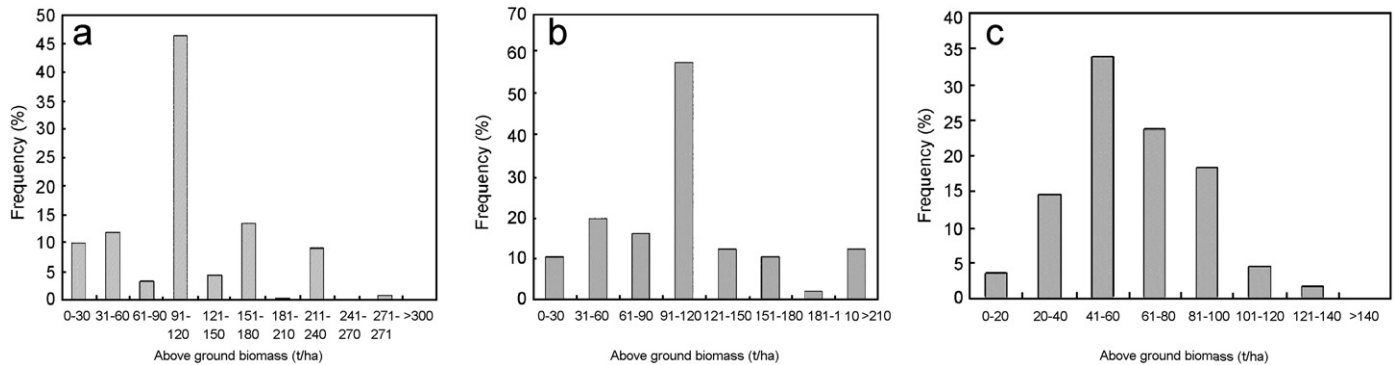


Fig. 8. Histogram of AGB frequency statistics.

AGB map, which was in turn created from the LAI map. In the final AGB mapping, maps of stand age, vegetation indices, and LAI were all used as the predictors of AGB. The information of vegetation indices may thus be over-used. The application of near infrared and shortwave infrared remote sensing data will reduce this limitation somewhat.

Terrain correction is especially important in processing remote sensing data for hilly areas like Liping County. The shadow effect imposes noise in remotely sensed signals. The reduction of the soil background effect by using RSR and the correction of the terrain effect improved the reliability of retrieved forest parameters.

In mountainous terrains, the accuracy of land cover classification based on  $ETM^+$  data is fairly low due to the heterogeneity of land surface within a  $30 \times 30$  m pixel. Dorren et al. (2003) added digital elevations as an extra band to improve the accuracy of Landsat  $ETM^+$ -based forest stand type mapping, and also compared the object-based classification with per-pixel classification. These authors divided forests into four types (dense conifer, open conifer, mixed forest and broadleaf). In our study, based on field investigations the supervised classification method was adopted to classify forests into different types; discrimination of forest species was not attempted because of the limitations of the Landsat  $ETM^+$  data. Although bamboo occupied about 1.94% of the land area in Liping County, it was scattered in many spots smaller than a  $ETM^+$  pixel ( $30 \times 30$  m). Any non-uniformity of vegetation distribution within a pixel of remote sensing imagery deteriorates the precision of AGB calculation.

Stand age served as an important and useful factor in estimating AGB. Leaf area remains almost the same once the stand age is above a threshold for forests in a similar environment while forest biomass continues to accumulate. The integration of stand age into an AGB model can to a large extent alleviate the underestimation of high AGB values. For regional applications, a robust method to infer stand age from remote sensing is required for reliable mapping of AGB.

## Acknowledgements

This study was supported by the Canada International Development Agency (CIDA). We are grateful to the help from Liping Forest Bureau during the field campaign.

## References

- Brown, L., Chen, J.M., Leblanc, S.G., Cihlar, J., 2000. A shortwave infrared modification to the simple ratio for LAI retrieval in boreal forests: an image and model analysis. *Remote Sensing of Environment* 71, 16–25.
- Chen, J.M., Cihlar, J., 1995. Plant canopy gap-size analysis theory for improving optical measurements of leaf-area index. *Applied Optics* 34, 6211–6222.
- Chen, J.M., Liu, J., Leblanc, S.G., Lacaze, R., Roujean, J.-L., 2003. Multi-angular optical remote sensing for assessing vegetation structure and carbon absorption. *Remote Sensing of Environment* 84, 516–525.
- Degui Gu, 1998. Topographic normalization of landsat TM images of forest based on subpixel Sun-Canopy-Sensor geometry. *Remote Sensing of Environment* 64, 166–175.
- Dorren, L.K.A., Maier, B., Seijmonsbergen, A.C., 2003. Improved Landsat-based forest mapping in steep mountainous terrain using object-based classification. *Forest Ecology and Management* 183, 31–46.
- Feng, Zongwei, et al., 1999. *Forest Ecosystem's Biomass and Productivity in China*. Science Press.
- Gitelson, A.A., 2004. Wide dynamic range vegetation index for remote quantification of biophysical characteristics of vegetation. *Journal of Plant Physiology* 161, 165–173.
- Goetz, S.J., Prince, S.D., Small, J., Gleason, A.C.R., 2000. Interannual variability of global terrestrial primary production: results of a model driven with satellite observations. *Journal of Geophysical Research-Atmospheres* 105, 20077–20091.
- Haripriya, G.S., 2000. Estimates of biomass in Indian forests. *Biomass and Bioenergy* 19, 245–258.
- International Panel on Climate Change (IPCC), 1996. *Climate change 1995. Impacts, adaptations and mitigation of climate: scientific-technical analyses. Contribution of Working Group II to the Second Assessment Report of the Inter-governmental Panel on Climate Change*. Cambridge University Press, Cambridge, UK.
- Jing-Yun, Fang, Geoff Wang guo-hua Liu, G., Xu, Song-Ling, 1998. Forest biomass of China: an estimate based of the biomass–volume relationship. *Ecological Applications* 8 (4), 1084–1091.
- Moreau, S., Le Toan, T., 2003. Biomass quantification of Andean wetland forages using ERS satellite SAR data for optimizing livestock management. *Remote Sensing of Environment* 84, 477–492.

- Prince, S.D., Goward, S.N., 1995. Global primary production: a remote sensing approach. *Journal of Biogeography* 22, 815–835.
- Rauste, Y., 2005. Multi-temporal JERS SAR data in boreal forest biomass mapping. *Remote Sensing of Environment* 97, 263–275.
- Running, S.W., Thornton, P.E., Nemani, R., Glassy, J.M., 2000. Global terrestrial gross and net primary productivity from the earth observing system. In: Sala, O.E., Jackson, R., Mooney, H.A., Hwarth, R. (Eds.), *Methods in Ecosystem Science*. Springer, New York, pp. 44–57.
- Spencer, R.D., Green, M.A., Biggs, P.H., 1997. Integrating eucalypt forest inventory and GIS in Western Australia. *Photogrammetric Engineering and Remote Sensing* 63, 179–181.
- Vermote, E.F., Tanre, D., Deuz, J.L., Herman, M., Morcrette, J.J., 1997. Second simulation of satellite signal in the solar spectrum.
- Vermote, E.F., Tanre, D., Deuze, J.L., Herman, M., Morcrette, J.J., 1997. Second simulation of the satellite signal in the solar spectrum, 6S: an overview. *IEEE Transactions on Geoscience and Remote Sensing* 35 (3), 675–686.
- Xu, Hui, 1999. A biomass model compatible with volume. *Journal of Beijing Forestry University* 21 (5), 32–36.
- Zhang, Jia-hua, Fu, Cong-bin, 1999. A study on relationships between remote sensing information and plant photo-synthetic parameters in estimating biomass model. *Acta Geodaetica et Cartographica Sinica* 28, 128–132.
- Zheng, D.L., Rademacher, J., Chen, J.Q., Crow, T., Bresee, M., le Moine, J., Ryu, S.R., 2004. Estimating aboveground biomass using Landsat 7 ETM+ data across a managed landscape in northern Wisconsin, USA. *Remote Sensing of Environment* 93, 402–411.